PCCP

RSCPublishing

ARTICLE

Anion resonances and above-threshold dynamics of coenzyme Q_0

Cite this: DOI: 10.1039/x0xx00000x

James N. Bull,[a] Christopher W. West[a] and Jan R. R. Verlet[a]

Received 00th January 2015,
Accepted 00th January 2015

DOI: 10.1039/x0xx00000x

www.rsc.org/

Temporary radical anions (resonances) of isolated co-enzyme Q_0 (CQ_0) and their associated above-threshold dynamics have been studied using frequency-, angle-, and time-resolved photoelectron imaging (FAT-PI). Experimental energetics and dynamics are supported with *ab initio* calculations. All results support that CQ_0 exhibits similar resonances and energetics compared with the smaller *para*-benzoquinone subunit, which is commonly considered as a prototype electrophore for larger biological *para*-quinone species. However, the above-threshold dynamics in CQ_0 relative to *para*-benzoquinone show significantly enhanced prompt detachment compared with internal conversion, particularly around the photoexcitation energy of 3.10 eV. The change in dynamics can be attributed to a combination of an increase in the shape character of the optically-accessible resonance at this energy, a decrease in the autodetachment lifetime due to the higher density of states in the neutral, and a decrease in the probability that the wavepacket formed in the Franck-Condon window can access the local conical intersection in CQ_0 over the timescale of autodetachment. Overall, this study serves as a clear example in understanding the trends in spectroscopy and dynamics in relating a simple prototypical *para*-quinone electrophore to a more complex biochemical species.

Introduction

Developing a comprehensive understanding of the spectroscopy and excited state dynamics of a particular class or series of complex biological molecules can be achieved by a bottom-up approach. By first developing an understanding of the key active centres, followed by systematically increasing molecular size or including the surroundings, deep insight into excited state processes can be gained. In most situations an increase in molecular size is accompanied with an increase in the number and density of accessible product channels, and consequently the detailed dynamics rapidly become very difficult to deconvolute with certainty.[1-4] Accordingly, the correct identification and study of prototypes can provide an important route to understanding the trends involved in building up to larger systems.

The quinone functional group is ubiquitous in nature and plays a central role in both biological and technological electron transfer chains.[5,6] Coenzyme Q_0 (2,3-dimethoxy-5-methyl-*para*-benzoquinone, Fig. 1), abbreviated hereafter as CQ_0, represents the smallest member of the coenzyme Q-series. The subscript refers to the number of isoprenyl subunits in an aliphatic tail attached to the unsubstituted position of CQ_0 (Fig. 1), which enhances lipid miscibility. The most common member is CQ_{10}, or ubiquinone, which is present in most eukaryote cells and participates in electron transport chain processes associated with aerobic respiration.[5,7-9] The quinone subunit acts as the electrophore in electron transfer processes.

We have recently used a combination of frequency-, angle-, and time-resolved photoelectron imaging (FAT-PI) to study the simplest *para*-quinone anion, *para*-benzoquinone (pBQ),[10,11] and also menadione (vitamin K_3),[12] which also is an active electron mediator in biology. Briefly, pBQ and its resonances has been the subject of several studies over the last few

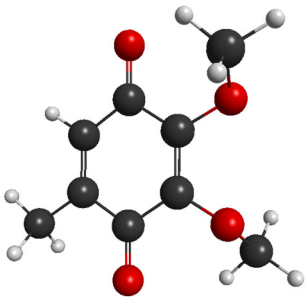

Fig. 1: Equilibrium geometry of the coenzyme Q_0 (CQ_0) radical anion Key: charcoal – carbon; red – oxygen; white – hydrogen.

decades. The majority of these studies have involved either electron attachment/transmission experiments or *ab initio* calculations with the principal aim of identifying the existence temporary anion resonances: a summary of the relevant literature can be found in West *et al*.[10] and Honda *et al.*[13]. We have recently developed the technique of FAT-PI spectroscopy in which resonances are prepared by photoexcitation of the ground electronic state radical anion. In ideal cases, FAT-PI can offer a higher degree of control of resonance preparation compared with electron attachment experiments, and can also allow the dynamics of selected above-threshold resonances to be tracked in real time. Overall, FAT-PI can provide a very complete and self-consistent account of temporary anion resonances and their dynamics in *para*-quinone species.[10,12]

Temporary anions or resonances are quasi-bound states that are energetically situated above the detachment threshold, with typical autodetachment lifetimes of tens to hundreds of femtoseconds.[14-17] Despite the transient existence of resonances, electronic internal conversion processes leading to delayed autodetachment from a lower-lying resonance can still compete with prompt autodetachment or, in ideal situations, a ladder of internal conversions may provide a route to form the ground electronic state of the anion.[12] Hence, certain resonances can act as doorway states to the formation of long-lived ground state anions. Resonances can generally be divided into two types: (i) shape resonances, in which an extra electron predominately occupies an unfilled valence orbital of the neutral ground electronic state configuration; and (ii) core-excited (or Feshbach) resonances, in which the corresponding neutral core is predominately in an electronically excited state.[14] Since autodetachment of a shape resonance only requires a one-electron transition in a Koopmans' interpretation, lifetimes are typically on the order of 10^{-14} s. In contrast, Feshbach resonances need a degree of electronic reconfiguration concerted with electron ejection to achieve the neutral electronic configuration and therefore exhibit longer autodetachment lifetimes (typically 10^{-13} to 10^{-12} s).

This paper reports a combined FAT-PI and *ab initio* electronic structure study on the radical anion resonances of CQ_0. Particular emphasis is placed on the comparison of the above-threshold dynamics with those characterised previously for the pBQ subunit. Briefly, similar to pBQ and menadione resonances,[10-12] CQ_0 shows is an interplay of four electron detachment processes: (i) direct photodetachment into the continuum; (ii) prompt autodetachment from an initially excited resonance; (iii) delayed autodetachment (DA), which corresponds to electron emission from excited states *after* some relaxation has occurred (either vibrational relaxation or internal conversion); and (iv) thermionic emission (TE), which is a statistical emission from the electronic ground state of the anion. Because the photoelectron spectra of (i) and (ii) cannot be resolved, these two channels are jointly termed prompt detachment (PD). In terms of electron kinetic energy (*eKE*) released, PD is larger than DA and TE peaks at *eKE* = 0 eV. The present study shows that the additional methyl- and methoxy-groups present in CQ_0 do little to modify the energies of the optically-active resonances because these involve $\pi^* \leftarrow \pi$ excitations, however, the branching ratios of autodetachment and above-threshold internal conversion are significantly modified.

Experimental

All FAT-PI experiments were performed using a photoelectron (PE) imaging spectrometer that has been described previously in detail.[12,18] Briefly, a ~1 mM solution of >99% purity CQ_0 (Sigma-Aldrich) dissolved in analytical grade methanol was electrosprayed and the resulting ions were transferred to vacuum *via* a capillary and into an RF ring-electrode ion trap. Ions were thermalized to ~300 K in the trap. The trapped ions were unloaded into a co-linear time-of-flight optics assembly in which the ion packet was accelerated along a 1.3 m flight region towards a continuous-mode penetrating field velocity-mapping (VMI) assembly.[19,20] Laser pulses were timed to interact with the mass-selected ion packet at the centre of the VMI stack. Ejected electrons were velocity-mapped onto a dual multichannel plate detector (MCP) followed by a P43 phosphor screen. Electron impacts were monitored by a CCD camera utilizing a ~500×500 pixel array. The *eKE* scale was calibrated from the spectrum of I^-, and the VMI resolution was ~5%. All VMI reconstructions used a polar onion peeling (POP)[21] algorithm that allows the PE spectrum and electron ejection angular distributions to be determined.

In the frequency- and angle-resolved experiments, PE images were collected at various wavelengths between $h\nu$ = 4.13 eV (300 nm) and $h\nu$ = 1.88 eV (660 nm), in 5, 10 or 20 nm increments. The tuneable radiation was generated by a Nd:YAG pumped (Continuum Surelite II-10) optical parametric oscillator (Continuum Horizon I). Each PE image accumulated sufficient counts to achieve a reasonable and comparable signal-to-noise ratio. All PE images were accumulated with a 500 ns gate on the MCP. The MCP gate allows collection of all prompt electron ejection, however captures only a small fraction (few percent) of thermionic emission, which occurs on a microsecond timescale.[12,22-25]

In the pump-probe time-resolved experiments, femtosecond laser pulses were derived from a Spectra Physics Ti:sapphire oscillator and regenerative amplifier. The 3.10 eV (400 nm, ~70 μJ) pump pulses were produced by frequency doubling of the 1.55 eV (800 nm) fundamental in a type I β-barium borate crystal. The 1.55 eV (800 nm, ~450 μJ) fundamental was used as the probe pulse. There was only a trace quantity of 400 nm two-photon signal. Pump and probe pulses were delayed relative to each other, Δt, using a motorised delay line. Both pulses were combined collinearly using a dichroic mirror, and were loosely focused into the interaction region using a curved metal mirror. Combined, the pump-probe cross-correlation has a full-width at half-maximum (FWHM) of ~80 fs, offering an ultimate time resolution of ~40 fs.

Computational

Ab initio calculations were performed using the GAMESS-US (May 2013 release) computational package.[26] All calculations used the aug-cc-pVDZ basis set,[27] although for computational tractability exclude the most diffuse set of *d* functions centred on carbon atoms. The modified basis set is denoted GEN1. Neutral CQ_0 has a calculated dipole moment of ~1.5 D, which does not support a dipole-bound anion.[28] The anion equilibrium geometry was optimised using frozen-core MP2 theory,[29] and confirmed to represent a geometrical minimum through vibrational frequency analysis. Using the optimised geometry, ground and excited state calculations were performed within the multi-state second-order XMCQDPT (extended multiconfigurational quasi-degenerate perturbation theory)[30] framework using (17,12) and (16,12) CASSCF reference wavefunctions and a denominator level shift of 0.02. That is, 17 or 16 active electrons distributed amongst 12 active orbitals for the anion and neutral, respectively. These active spaces include all π and π* molecular orbitals as well a set of lone pair orbitals for each oxygen atom.† Oscillator strengths were computed within the CAS-CI framework. All relevant zero point energies were included and were scaled by a factor of 0.98.[31] CCSD(T)/GEN1 calculations at the MP2 geometries were performed using the Gaussian 09 computational package.[32,33]

It is noted that the optically-dark 1^2B_{3u} resonance of pBQ first identified in the SAC-CI + Rydberg orbital calculations of Nakatsuji and co-workers[13] and subsequently in our earlier XMCQDPT2 calculations,[10] is a mixed valence-diffuse state, and changes considerably in character and energy in transitioning from the neutral to anion geometries.[10,12] While for pBQ, this resonance was required to describe electron attachment experiments (at the neutral geometry), in CQ_0 this optically-dark resonance has behaviour resembling a discretised continuum state, and is therefore unlikely to play any significant role in the spectroscopy and dynamics.

Conical intersections between the 5^2[F] and 3^2[S] resonances (2^2B_{3u} and A_u for pBQ; 'F' and 'S' are defined below) were located using state-averaged CASSCF wavefunctions with the non-adiabatic coupling matrix element algorithm as implemented in GAMESS-US.[34] Once the conical intersection geometries were located, their respective energies were computed using the multi-state XMCQDPT method.

Franck-Condon simulations of the direct photodetachment spectrum were performed at the ωB97XD//GEN1 level of theory in the harmonic approximation.[35] Boltzmann population temperature contributions were included at 300 K.

Results and Analysis

Frequency- and angle-resolved PE spectroscopy

Photoelectron (PE) spectra at three selected *hv* are given in Fig. 2 along with the corresponding spectra for the pBQ subunit taken from West *et al.*[10]. Each spectrum is normalised such that its total intensity is unity. It is immediately evident that there is very good agreement between the CQ_0 and pBQ anion spectra at *hv* = 4.13 eV, implying similar electron ejection processes. At *hv* = 3.10 eV, which is close to being resonant with photoexcitation to analogous Feshbach resonances in both CQ_0 and pBQ, the PE spectra indicate different yields of prompt (high-*eKE*) *vs* delayed (low-*eKE*) electron ejection. There is also a reduced contribution of thermionic emission (ground state statistical ejection), which occurs in the *eKE* < 0.1 eV

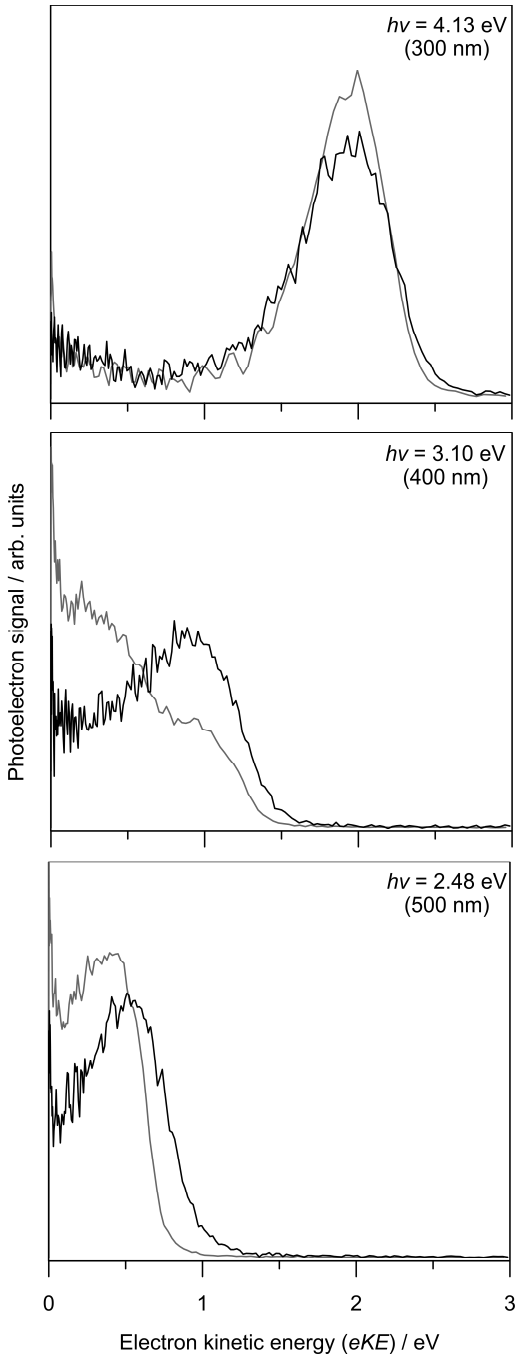

Fig. 2: Selected CQ_0 anion photoelectron spectra. Included in grey are the corresponding pBQ anion photoelectron spectra at the same photon energy (taken from Ref. 10). All spectra have been normalised to a total photoelectron yield of unity.

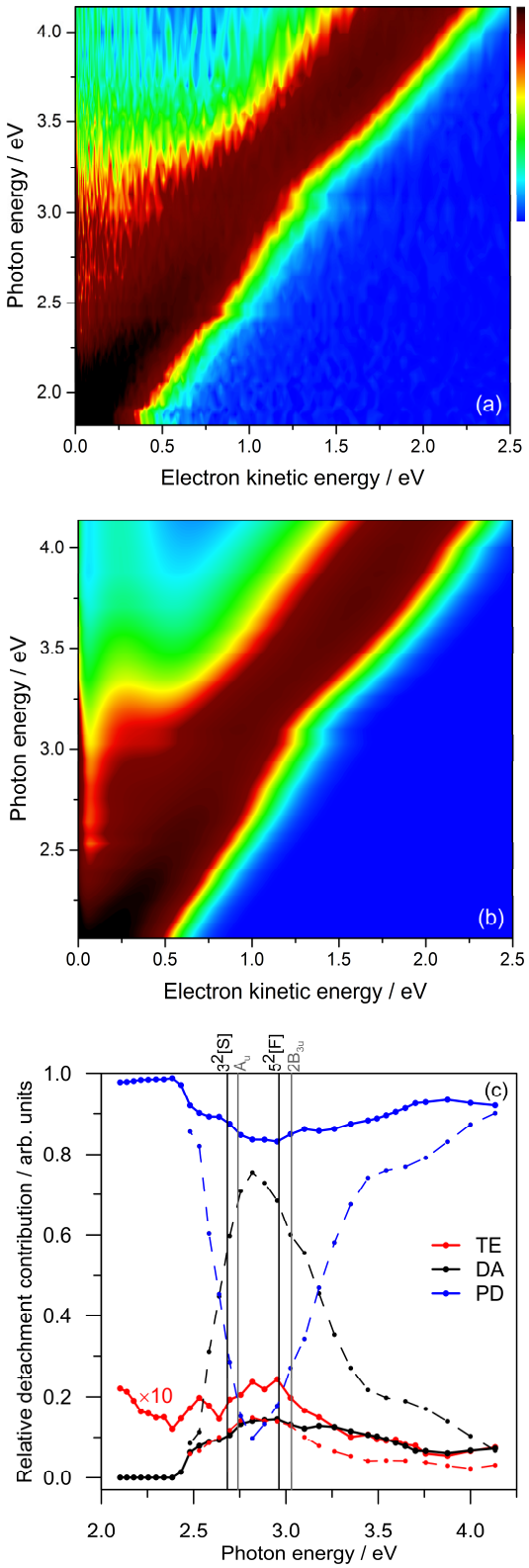

Fig. 3: (a) frequency-resolved photoelectron spectra of the CQ_0 anion; (b) globally-fitted model of experimental data; and (c) relative contributions of each electron ejection channel from model fit for CQ_0 (solid) and pBQ (dashed). Note that the TE contribution for CQ_0 has been scaled by 10-fold. Key: TE – thermionic emission; DA – delayed autodetachment; PD – prompt detachment.

window. At hv = 2.48 eV, the CQ_0 spectrum is again very similar to that for pBQ. Finally, in all three spectra it is evident that CQ_0 produces photoelectrons reaching a slightly higher upper-bound in *eKE* than pBQ, which may indicate that CQ_0 has a slightly lower adiabatic electron affinity than pBQ.

Fig. 3a summarises all 40 frequency-resolved PE spectra, normalised to unit total intensity. All individual spectra are given in the ESI.† A number of trends are immediately obvious: (i) at the three lowest hv (1.91 eV, 1.88 eV, 1.82 eV), the PE spectra are essentially identical; (ii) the predominant electron ejection channel(s) across the entire hv range produce electrons with high *eKE*; and (iii) at all hv there is a small yield of electrons with *eKE* < 0.5 eV, although above hv ~ 3.6 eV this channel is significantly reduced.

In a similar vein to the recent analysis of menadione,[12] Fig. 3b was produced by a globally-fitted model of the frequency-resolved PE spectra. The fitting procedure involved a number of assumptions: (i) the thermionic emission (TE) contribution is described by a single Richardson-like function with internal temperature correlating with internal energy (c.f., increasing hv);[25] (ii) the delayed autodetachment (DA) feature assumes a Gaussian distribution convoluted with a Wigner threshold expression near zero *eKE* (assuming l ~ 0);[36,37] (iii) all spectral parameters such as the *eKE* centres and spectral widths of the DA and PD features are shared and constant across all PE spectra – with the exception that the PD distribution centre in *eKE* space increased linearly with hv (i.e., fixed in electron binding energy). Each of these detachment channels are defined and described in detail in the following discussion section. The final fit was that requiring the minimum number of basis functions that reproduces the experimental data in good accord, and without any significant systematically unassigned residual (see ESI).† The relative areas of each of the three modelled detachment channels are given in Fig. 3c as a function of hv. For hv < 2.1 eV, distinct PE features are not sufficiently resolved to fit. Also included in Fig. 3c, for comparison, are the analogous contributions from pBQ by applying a similar global fitting model to the frequency-resolved PE spectra in West *et al.*[10] – further details are given in the ESI.†

Fig. 4 summarises the electron ejection anisotropy associated with the frequency-resolved PE spectra given in Fig. 3a in terms of the conventional β_2 parameter.[38] Two regions, (i) and (ii), are identified in Fig. 4 with β_2 values averaged over these regions of +0.10 and –0.16, respectively. Positive and negative β_2 corresponds to electron ejection parallel and perpendicular to the laser polarization, respectively. Changes in electron angular ejection or image anisotropy over regions of the frequency-resolved PE spectra indicates a change in either the electronic character of autodetachment or a change in electron ejection mechanism, e.g., autodetachment *vs* direct photodetachment.[10,12,39]

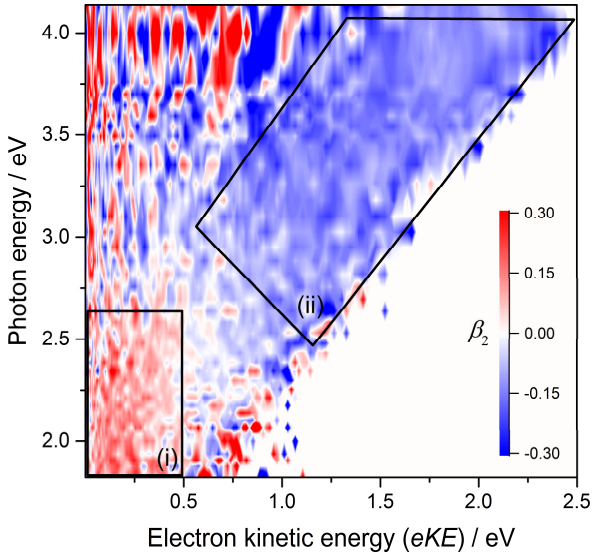

Fig. 4: CQ_0 anion electron ejection angular anisotropy (β_2). Two regions, (i) and (ii), have been identified and are discussed in the text. Note that a five-point moving-mean has been applied to all β_2 data in this figure.

Time-resolved PE spectroscopy

The 3.10 + 1.55 eV (400 + 800 nm) time-resolved measurements are summarised in Fig. 5. The pump pulse photoexcites the resonance at hv ~3.10 eV, and the probe pulse monitors the above-threshold population in real time. Fig. 5a shows two representative pump-probe spectra: Δt = ±500 fs, which is identical to the 3.10 eV femtosecond PE spectrum; and Δt = 20 fs, which shows the pump-probe signal between 1.6 < *eKE* < 3.0 eV and a corresponding depletion in the prompt detachment peak centred at *eKE* ~ 0.9 eV. Inset in Fig. 5a, the pump-probe feature is approximately divided into contributions from the two resonances involved in the dynamics: nascent photoexcited 5^2[F]; and the lower-lying 3^2[S] resonance produced following internal conversion. Fig. 5b shows the relative populations (signal integrals) of each resonance as a function of Δt. The time-varying populations were fitted to Gaussian cross-correlation functions convoluted with exponential decays (and rise for 3^2[S]). The dynamics appear to be limited by the experimental cross-correlation.

Ab initio calculations

The *ab initio* energetics are summarised in Fig. 6, and are compared with earlier calculations on the pBQ subunit.[10] Each above-threshold resonance has been labelled by its predominant character: 'S' for shape; and 'F' for Feshbach. Also included in Fig. 6 in parentheses are the calculated photoexcitation oscillator strengths for both CQ_0 and pBQ, all determined at the same level of theory. Table 1 summarises the CASSCF configuration weights of overall shape and Feshbach character of each resonance.

From Fig. 6 it is immediately obvious that the respective resonance energetics and photoexcitation oscillator strengths are very similar between CQ_0 and pBQ, although from Table 1 the relative character of the resonances has changed. In particular, the optically-active ^2A_u resonance in pBQ has increased in Feshbach character in CQ_0, while the 2^2B_{3u} resonance has increased in shape character. From Table 1 alone one might, to a first approximation, expect reasonable similarity between the experimental resonance energetics, although an increased affinity for prompt autodetachment at hv ~3.10 eV due to the increased shape character of the optically-active resonance at this energy. Because all resonances involve excitation to π* orbitals, and all groups attached to the *para*-quinone ring are saturated and only weakly interacting, the resonance energtics are very close to those in pBQ.

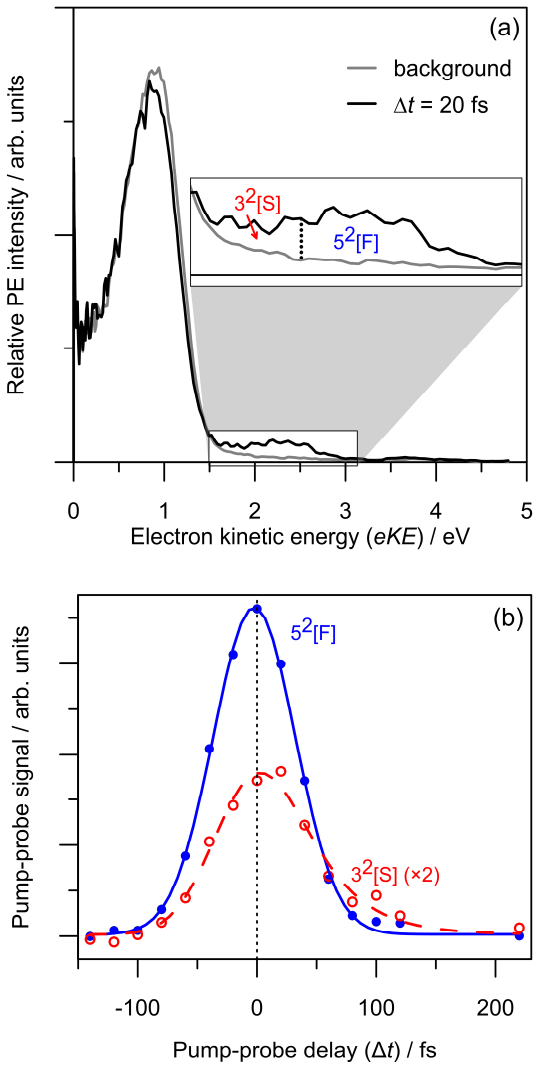

Fig. 5: 3.10 + 1.55 eV (400 + 800 nm) pump-probe time-resolved PE of the CQ_0 anion. (a) Two example spectra at Δt = ±500 fs and 20 fs; the former is considered as the background. The inset highlights the pump-probe signal, which is divided into the contributions from two resonances. (b) Relative populations of each resonance as a function of pump-probe delay, Δt. Solid (blue) and dashed (red) lines are fits of the integrated 5^2[F] and 3^2[S] PE signal, respectively. The 3^2[S] signal has been scaled by a factor of two.

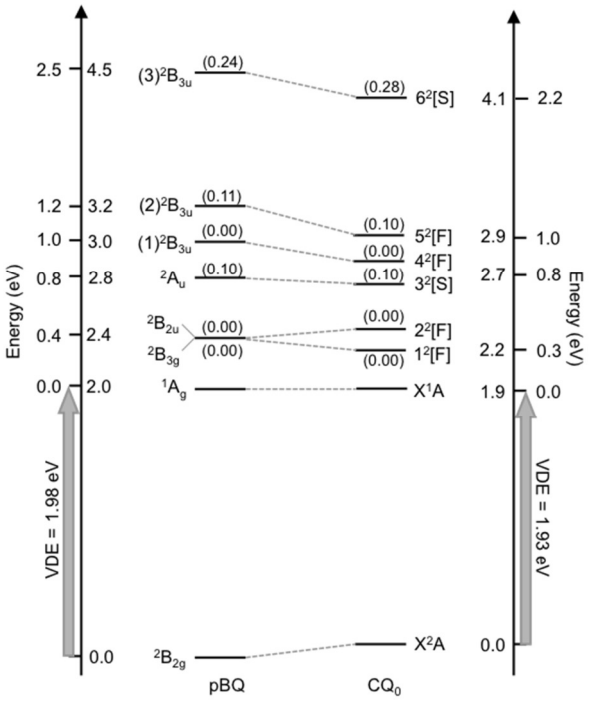

Fig. 6: Calculated energetics of CQ_0 (right) compared with the pBQ (left) using XMCQDPT2 theory. All calculations assume the ground anion state geometry. VDE is the anion vertical detachment energy. Included in parentheses are calculated excitation oscillator strengths. The inner/outer energy axis is relative to the neutral/anion ground state.

The adiabatic electron affinity (AEA) and vertical detachment energy (VDE) of the anion were calculated to be AEA = 1.51 eV and VDE = 1.88 eV from the multireference wavefunctions. For comparison, the CCSD(T)/MP2 calculated values were AEA = 1.52 eV and VDE = 1.79 eV. For pBQ, electron affinities were previously calculated at AEA = 1.85 eV and VDE = 1.98 eV using the CCSD(T)//aug-cc-pVTZ level of theory, which supports the experimental result that the AEA is slightly lower in CQ_0.[10] Finally, the two lowest energy resonances are of nπ* Feshbach character and involve excitation from oxygen lone pair *p* orbitals to π* orbitals. These resonances are essentially optically-dark and, similar to pBQ,[10,11,40] appear to play little role in the above-threshold dynamics of CQ_0.

Discussion

The combined experimental results and ab initio calculations allow a detailed account of the temporary anion resonances and above-threshold dynamics to be developed. In particular, there are close correspondences in the spectroscopy of the resonances, although key differences in above-threshold detachment probabilities (dynamics) compared with the isolated pBQ subunit are also apparent.

Table 1: CASSCF weights (in percent) of shape, S, and Feshbach, F, character of each temporary anion resonance in pBQ and CQ_0 assuming the geometry of the ground electronic state anion.

Resonance label in pBQ/CQ_0	pBQ	CQ_0
$^2B_{1g}$ / 1^2[F]	100% F	100% F
$^2B_{2u}$ / 2^2[F]	100% F	100% F
^2A_u / 3^2[S]	91% S, 9% F	62% S, 38% F
2^2B_{3u} / 5^2[F]	19% S, 81% F	41% S, 59% F
3^2B_{3u} / 6^2[S]	57% S, 43% F	45% S, 55% F

Electron detachment channels

From Fig. 3a, the PE spectra at the three lowest *hv*, which were noted to be essentially identical, can be attributed to vibrational autodetachment.[17,41,42] Vibrational autodetachment arises when the anion has vibrational energy in excess of the binding energy of its most weakly bound electron, and vibratory motion that modulates the orbital in which the most weakly electron resides shakes off the election. Timescales range from 100s femtoseconds to microseconds. PE signal rapidly diminished at *hv* lower than that plotted in Fig. 4, indicating that the internal vibrational temperature is on the order of a few hundred meV. Assuming a harmonic partition function, our vibrational frequency calculations indicate ions thermalised to 300 K would contain 280 meV of internal vibrational excitation, supporting the above assignment.

All frequency-resolved PE spectra with $hv > 2.0$ eV have most intensity associated with the production of high-*eKE* electrons, the *eKE* of which increases with *hv*. Such electrons are consistent with the combination of instantaneous direct photodetachment into the neutral continuum and photoexcitation followed by prompt autodetachment (i.e., autodetachment before any other above-threshold non-adiabatic dynamics may occur, typically < 20 fs). Because our experiment cannot distinguish between these two processes, they are jointly considered as prompt detachment (PD). Indeed, the model fit in Fig. 3b and corresponding channel contributions in Fig. 3c quantify that PD is > 80% of the PE signal across all *hv*. From $hv > 2.5$ eV, photoelectrons distinct from the high-*eKE* diagonal of PD can be identified in the *eKE* range of $0.1 < eKE < 0.5$ eV, which result from delayed autodetachment (DA) processes.

From the PE anisotropy in Fig. 4, region (i) with average $\beta_2 = +0.10$ arises from the combination of direct photodetachment and autodetachment of the photoexcited 3^2[S] resonance. For *hv* >2.5 eV, the β_2 value over the $0.1 < eKE < 0.5$ eV window averages to approximately zero, suggesting a change in detachment mechanism. The change coincides with photoexcitation of the 5^2[F] resonance. Similar to pBQ, the change of β_2 can be interpreted as an internal conversion from

the 5^2[F] to 3^2[S] resonances, from which the electron is subsequently ejected to contribute to the $0.1 < eKE < 0.5$ eV window.[10] For $h\nu > 2.75$ eV, the β_2 on the PD diagonal, identified as region (ii) in Fig. 4, has changed sign compared with that in region (i), reflecting a change in the detachment character. For $3.70 < h\nu < 4.13$ eV, photoexcitation is resonant with the 6^2[S] resonance. The 6^2[S] resonance is strongly optically-allowed compared with the lower energy resonances. Electron ejection is predominantly by PD, which is consistent with both the shape character of this resonance, and the large separation in energy with other resonances meaning that internal conversion is less likely. The change in photoexcitation from the 5^2[F] to 6^2[S] resonance does not yield a change in β_2. In general, a sudden change in $\beta_2(h\nu)$ indicates a different detachment process, however, the lack of a change in $\beta_2(h\nu)$ does not reflect the lack of a change in detachment process.

The small contribution of PE signal at $eKE \sim 0$ eV across all frequency-resolved PE spectra is assigned to thermionic emission (TE). TE arises from internal conversion(s) to form the ground electronic state anion, which statistically detaches the excess electron over a long timescale (tens to hundreds of microseconds).[12,22-25] The small contribution of TE in Fig. 3c for both CQ_0 and pBQ parallels the PD trend, which supports that the 3^2[S] resonance acts as an intermediate state in the sequence of above-threshold relaxation dynamics to achieve the ground electronic state.

From the global fit of the PD feature in Fig. 3b, the VDE is determined at 1.93(4) eV and the AEA at 1.60(6) eV. These electron affinities are in good agreement with the multi-reference perturbation theory values (CCSD(T)/GEN1 in parentheses) at VDE = 1.93 eV (1.96 eV) and AEA = 1.52 eV (1.52 eV). For pBQ, the global model fit yielded a VDE = 1.99(4) eV and AEA = 1.82(6) eV. These values are in excellent agreement with high-resolution photodetachment data from Schiedt and Weinkauf[40] (AEA = 1.860(5) eV), and our earlier CCSD(T)//aug-cc-pVTZ calculations at VDE = 1.98 eV and AEA = 1.85 eV.[10] These data support the result identified from Fig. 2 that the AEA of CQ_0 is ~0.25 eV lower than that for pBQ, while the experimental VDE of CQ_0 and pBQ agree within combined experimental error. In addition, the VDE for CQ_0 is difficult to determine because there is substantial overlap of the prompt autodetachment and direct photodetachment contributions in the PD feature. To our knowledge, there are no other known experimental determinations of electron affinity parameters for any co-enzyme Q species.

As a check that the global fitting procedure can reasonably account for PD spectrum, we have computed the harmonic ωB97XD//GEN1 Franck-Condon photodetachment spectra of both pBQ and CQ_0, which are shown in Fig. 7. The calculation is convoluted with a vibrational FWHM of 500 cm^{-1} (~62 meV), which is comparable with the experimental imaging resolution of ~5%. The Franck-Condon spectra are given in terms of electron binding energy (*eBE*), which is determined from any given PE spectrum by: $eBE = h\nu - eKE$. In accord with the present PE spectra and also pBQ anions cooled to 70 K, there is no clear vibrational structure.[43] The calculated Franck-Condon spectrum for pBQ is in very good agreement with the globally fitted PD feature. At high *eBE*, the Franck-Condon simulation predicts less PE signal than that fitted, which is in part attributed to the neglect of anharmonic effects in the calculations. For CQ_0, the array of anion conformations that can be accessed at 300 K has significantly increased. At 300 K CQ_0 has 280 meV of internal vibrational energy while pBQ has 90 meV. Our Franck-Condon calculations only consider the global ground anion and neutral conformations and different conformations will broaden the calculated distribution. In addition, anharmonic contributions at higher *eBE* become increasingly important for CQ_0 due to the increased number of lower frequency vibrational modes. These factors will result in a smearing of the experimental CQ_0 PE spectrum compared with that calculated. Finally, we note that the above comparison of calculated direct photodetachment with experimentally-fitted PD spectra assumes that the spectral shape of the prompt autodetachment component as a function of *eBE* parallels that of direct photodetachment. However, this assumption can break down because of Franck-Condon factors for resonant excitation followed by prompt autodetachment being different to those of direct photodetachment.

The time-resolved data of Fig. 5 demonstrate that the above-threshold dynamics are very fast and are essentially limited by the experimental femtosecond pulse cross-correlation. The divide between the 3^2[S] and 5^2[F] resonance contributions, shown in Fig. 5a, was selected considering the frequency-resolved experiments and *ab initio* calculations, translated by the probe energy. The PE signal decay from the 5^2[F] resonance in Fig. 5b results from the combination of prompt autodetachment and internal conversion. The integrated signal

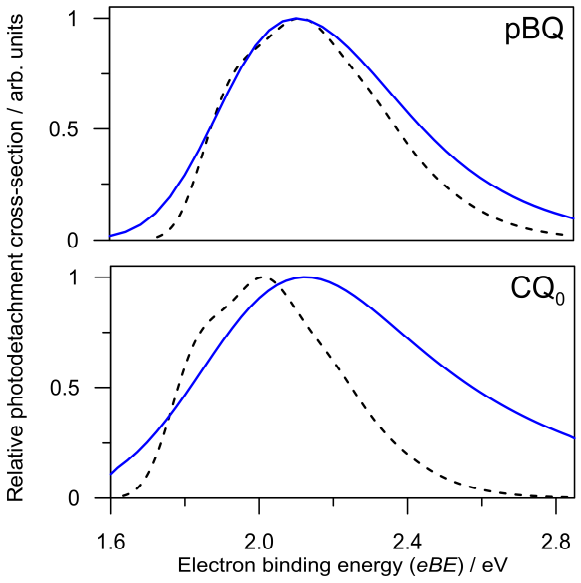

Fig. 7: Harmonic ωB97XD/GEN1 Franck-Condon photodetachment simulation at 300 K (black lines) compared with the globally-fitted prompt detachment feature from the frequency-resolved spectra (blue lines). The calculation assumes only the lowest energy conformations for CQ_0.

shows that the 3^2[S] population is slightly delayed relative to that of 5^2[F], which supports that photoexcited 5^2[F] population is internally-converted into the 3^2[S] resonance. We note that the total intensity of the 5^2[F] resonance in Fig. 5b is approximately three times that of the 3^2[S] resonance, which is consistent with the frequency-resolved measurements that PD (prompt autodetachment in the pump-probe experiment) is much more efficient than internal conversion. However, it is difficult to quantify the time-resolved populations with certainty because the pump-probe contributions of each resonance are considerably overlapped, and one must assume that the probe photodetachment cross-sections of each populated resonance are approximately equal. Overall, the time-resolved experiments support the contention that most of the photoexcited 5^2[F] resonance population autodetaches, while only small amount internally-converts and subsequently autodetaches. All above-threshold dynamics occur on a < 40 fs timescale. Note that the 3^2[S] could decay by further internal conversion *via* two lower-lying nπ* resonances, however, we see no evidence for such in the time-resolved spectra.

Comparison with *para*-benzoquinone

The experimental FAT-PI trends outlined above are similar to those recently established for pBQ anions.[10] As a comparison, the frequency-resolved spectra of pBQ as well as the global model plotted on the same intensity scale as CQ_0 are given in the ESI.† The relative contributions of the TE, DA and PD channels have been included in Fig. 3c. Note that we cannot directly compare the measured contribution of TE within the MCP gate from CQ_0 with pBQ because the former can statistically store more internal energy amongst its vibrational modes, which will likely result in an increased TE lifetime.

The observed β_2 trends for CQ_0 are also analogous with those for pBQ. However, the low point symmetry of CQ_0 combined with the increase in the number of available conformations at 300 K probably results in a reduction of β_2. Region (i) in Fig. 4 has an averaged β_2 of +0.10, which compares with that from pBQ at +0.20, and region (ii) has an averaged β_2 of –0.16, compared with –0.5 to –0.6 in pBQ. Comparison of region (ii) with that for pBQ further supports that the PD feature is spectrally broader in CQ_0.

The time-resolved experiments show a similar sequence of above-threshold dynamics in CQ_0 compared with pBQ, although, in agreement with the frequency-resolved measurements, different efficiencies of PD and DA. That is, some of the initial 5^2[F] population internally converts into 3^2[S] population, which in turn autodetaches. We have characterised the lifetime of both 5^2[F] and 3^2[S] resonance population to be sub-40 fs, which is similar to that for pBQ.[11]

Overall, both CQ_0 and pBQ exhibit analogous temporary anion resonances although, as first identified from the $h\nu$ = 3.10 eV spectrum in Fig. 2, the above-threshold dynamics have changed to yield a significant decrease in DA compared with PD for CQ_0. There are three possible mechanisms, or combinations thereof, for this apparent change in above-threshold dynamics: (i) prompt autodetachment occurs on a shorter timescale for 'larger' CQ_0 by virtue of an increase in the neutral vibrational state density and/or increase in shape resonance character; (ii) the rate of internal conversion is kinetically slower in CQ_0 compared with pBQ; and (iii) direct photodetachment into the neutral continuum is more competitive than photoexcitation in CQ_0 compared with pBQ at $h\nu$ = 3.10 eV.

Mechanisms (i) and (ii) can be further identified using *ab initio* calculation of resonance character and local conical intersections as discussed in the next section. Mechanism (iii) is more difficult to quantify without a comprehensive theoretical framework that is beyond the scope of the present study. However, we can hypothesise that mechanism (iii) is unlikely based on experimental trends of total PE yield across other related systems and electron attachment experiments of related species.[44] For example, both CQ_0 and pBQ have similar: electronic structure, geometries, electron affinities, resonances and calculated oscillator strengths; and only one accessible neutral detachment continuum. In addition, we did not observe any sudden changes in the β_2 parameters that would support a sudden increase in the relative contributions. Further, Fig. 3c shows no sudden changes in the contributions of PD *vs* DA for photon energies around 3.10 eV. Finally, in a series of electron attachment/transmission experiments considering a range of substituted *para*-quinones,[45] it is noted that saturated constituents do not significantly alter either the total scattering cross-sections or the number of resonance features as a function of electron energy.

Efficiency of autodetachment and internal conversion

In order to understand the relative contributions of mechanisms (i) and (ii), we consider further *ab initio* calculations. From Table 1, we identified that the resonance photoexcited at $h\nu$ = 3.10 eV has significantly increased shape character in CQ_0 compared to that in pBQ. It is both experimentally well-established and consistent with a Koopmans' interpretation that shape resonances typically have shorter lifetimes than Feshbach resonances by virtue of decreased electronic reorganisation in order to reach the neutral electronic state. Moreover, in accord with the Fermi golden rule, an increase in molecular size results in an increase in the density of vibrational states and, consequently, autodetachment lifetimes may be expected to decrease. Faster rates of autodetachment mean that other above-threshold dynamics are not as kinetically competitive. Thus, mechanism (i) will likely be an important contribution to the increased PD in CQ_0 compared with pBQ at $h\nu$ = 3.10 eV. We note that comprehensive theoretical frameworks can be used to predict autodetachment lifetimes, for example, like that recently applied to the ^2A_u shape resonance in pBQ,[46] however such considerations are beyond the scope of the current work.

The influence of mechanism (ii) is inferred by considering the calculated conical intersections for CQ_0 (5^2[F]/3^2[S]) and pBQ ($^2B_{3u}/^2A_u$), which are summarised in Fig. 8. All calculations considered CASSCF(13,10) geometry optimisation followed by a XMCQDPT2 energy calculation. The $^2B_{3u}/^2A_u$ conical intersection found here is in very good agreement with

that calculated in pBQ previously using a CASSCF(9,8) optimization followed by a CASPT2 energy calculation.[11] The predominant geometrical change to reach the conical intersection in pBQ involves a stretching of the C=C ring and the C=O bonds. While the energy of the ^2A_u state is given at the ground electronic state geometry, the energy of the ^2A_u resonance in its equilibrium geometry is only 0.1 eV different.[10,11] For CQ_0, while the changes in geometry to reach the 5^2[F]/3^2[S] conical intersection are similar to those involved in pBQ, the relative energy of the conical intersection is slightly above that of the 5^2[F] resonance onset. In addition, the conical intersection coupling strength compared with pBQ has decreased. Overall, we expect that the initial photoexcited wavepacket at *hv* ~3.10 eV will, on average, take longer to achieve the internal conversion in CQ_0 compared with pBQ.

In summary, we conclude that mechanism (ii) can also contribute to the increased PD in CQ_0 compared with pBQ at *hv* = 3.10 eV. Unfortunately, we cannot disentangle the relative importance of mechanism (i) and (ii). However, from the time-resolved experiments it is clear that the internal conversion process in both pBQ and CQ_0 both occur on a < 40 fs timescale, which places an upper limit on the above-threshold non-adiabatic timescales.

Finally, the small quantity of TE observed at wavelengths around *hv* = 3.10 eV is considered. In our earlier studies on pBQ, the TE contribution was postulated to result from a sequence of internal conversions involving the ^2A_u resonance as an intermediate. The idea of a ladder sequence of internal conversions was further supported in the study of menadione in which TE is the predominant electron ejection mechanism at all photoexcitation energies.[12] Returning to pBQ, while Horke *et al.*[11] identified a direct conical intersection between the 2^2B_{2u} resonance and ground electronic state, the conical intersection involves considerable distortion of the quinone ring out of plane to a C_{2v} geometry, which was considered unlikely on the < 40 fs timescales. The situation will probably be similar for CQ_0, and thus the small quantity of TE observed at photoexcitation energies of around *hv* = 3.10 eV will likely be produced *via* internal conversion first to the intermediate 3^2[S] resonance (^2A_u in pBQ), and subsequent internal conversion to the ground electronic state. As noted earlier, the global model of the frequency-resolved experiments support that the 3^2[S] (^2A_u in pBQ) acts as an intermediate in production of the TE signal because the relative contribution of TE parallels that of DA (see Fig. 3c).

An alternative mechanism that should be considered is the proposal of Khovstenko *et al.*[47,48] in which selected resonances of doublet spin multiplicity can undergo an intersystem crossing to form a long-lived quartet resonance. The mechanism was originally proposed to explain what the authors termed 'anomalously long-lived anions' that detach electrons (of unknown kinetic energy) on a microsecond timescale. From our FAT-PI experiments, albeit starting at the ground state

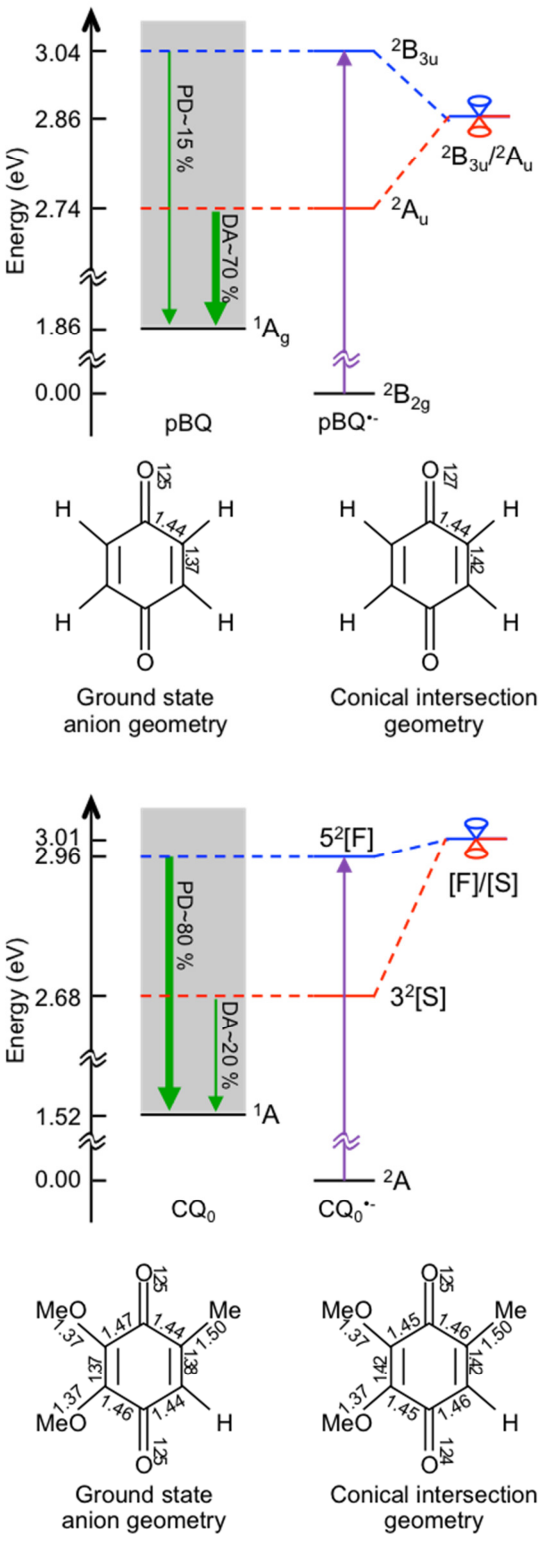

Fig. 8: Schematic summary of pBQ (upper) and CQ_0 (lower) above-threshold internal conversion dynamics assuming photoexcitation of the resonance at *hv* ~3.10 eV. Also shown are the respective geometries of the ground state anion and at the conical intersection.

anion geometry rather than the neutral geometry, we have not observed any experimental evidence of such a mechanism. We have, however, observed long-lived ground state anions. In our experiments, the decay of long-lived anions were unequivocally assigned to result from the process of TE based on monitoring electronic state populations in real-time and characterising the *eKE* distribution of photoelectrons. The recent study of menadione provides the clearest example of TE,[12] where it was established that the lowest quartet resonance in the adiabatic limit is situated *above* the photoexcited resonances.

Conclusions and outlook

This paper has characterised a number of temporary radical anion resonances of co-enzyme Q_0 (CQ_0) and their respective above-threshold dynamics using frequency-, angle-, and time-resolved photoelectron imaging (FAT-PI) and *ab initio* electronic structure calculations. The spectroscopy and dynamics of these resonances are analogous to those established for the simplest *para*-benzoquinone (pBQ) electrophore subunit, although the detailed above-threshold dynamics are different. In particular, CQ_0 shows significantly enhanced prompt detachment (high-*eKE* electrons) compared with internal conversion followed by delayed autodetachment (low-*eKE* electrons), particularly around the photoexcitation energy of 3.10 eV (400 nm). The change in dynamics is attributed to the combination of: (i) an increase in the shape character of the optically-accessible resonance at $h\nu \sim 3.10$ eV, leading to an increase in the prompt autodetachment rate; and (ii) a decrease in the kinetic probability that the wavepacket on the excited state can access the required local conical intersection for internal conversion. We noted in the introduction that CQ_0 is the simplest co-enzyme species and differs from the ubiquitous CQ_{10} by a long non-conjugated aliphatic side chain. The difference in side chain is similar to the difference between vitamin K_3 (menadione) and vitamin K_1, where we have shown that the presence of the aliphatic chain has very little influence on the photoelectron spectra.[12] It is not unreasonable to assume the same for the co-enzyme species. Finally, we note that the *para*-quinone moiety is also important in artificial electron acceptors, which show similar ultrafast internal conversion dynamics when the electron loss channel is closed.[49,50]

Overall, this study has helped develop an understanding of how the dynamics of resonances in the pBQ
prototype electrophore can be correlated to the dynamics to a more complex biochemical species. In addition, this study serves as an excellent example of the high degree of both spectroscopic specificity and selectivity that can be achieved using the FAT-PI technique. In particular, FAT-PI is well-suited to study 'larger' molecular anions formed through electrospray, because the technique is universal with molecular size. That is, anions of hundreds to thousands of atomic mass units can be readily prepared in the gas-phase and photoelectron spectroscopy is sensitive to only the most weakly bound electrons or frontier orbitals. Moreover, the technique is not restricted to resonances of open-shell anions, for example, as recently demonstrated in characterising the dynamics of the green fluorescent protein chromophore following UV excitation.[51,52]

Finally, while studies in the gas-phase provide the ultimate selectivity in spectroscopy and dynamics, this environment is alien compared with the solution or condensed phases present in actual biochemical systems. The next step is to understand how the incorporation of intermolecular interactions (e.g., hydrogen-bonding, solvation, etc.) modifies the *para*-quinone gas-phase dynamics and trends.

Acknowledgements

Funding was provided by the ERC (Starting Grant 306536).

Notes and references

[a]Department of Chemistry, Durham University, South Road, DH1 3LE, United Kingdom.

† Electronic Supplementary Information (ESI) available: summary of the global-fitting model for pBQ and fitting residuals; π and π* molecular orbitals included in the CASSCF active space; and plots of all photoelectron spectra included in Fig. 3a. See DOI: 10.1039/b000000x/

[1] R. D. Levine, Molecular Reaction Dynamics, Cambridge University Press, 2009.

[2] N. E. Henriksen and F. Y. Hansen, Theories of Molecular Reaction Dynamics: The Microscopic Foundation of Chemical Kinetics, Oxford University Press, 2012.

[3] P. L. Houston, Chemical Kinetics and Reaction Dynamics, Dover Publications, 2006.

[4] T. Baer and M. Mayer, *J. Am. Soc. Mass Spectrom.,* 1997, **8**, 103.

[5] B. Nowicka and J. Kruk, *Biochim. Biophys. Acta,* 2010, **1797**, 1587, 2010.

[6] B. L. Trumpower, Ed., Function of Quinones in Energy Conserving Systems, Academic Press, 1982.

[7] M. Turunen, J. Olsson and G. Dallner, *Biochim. Biophys. Acta,* 2004, **1660**, 171.

[8] G. Lenaz, R. Fato, G. Formiggini and M. L. Genova, *Mitochondrion,* 2007, **7S**, S8.

[9] M. L. Genova and G. Lenaz, *BioFact.,* 2011, **37**, 330.

[10] C. W. West, J. N. Bull, E. Antonkov and J. R. R. Verlet, *J. Phys. Chem. A,* 2014, **118**, 11346.

[11] D. A. Horke, Q. Li, L. Blancafort and J. R. R. Verlet, *Nat. Chem.,* 2013, **5**, 711.

[12] J. N. Bull, C. W. West and J. R. R. Verlet, *Chem. Sci.,* 2015, **6**, 1578.

[13] Y. Honda, M. Hada, M. Ehara and H. Nakatsuji, *J. Chem. Phys. A,* 2002, **106**, 3838.

[14] H. S. Taylor, G. V. Nazaroff and A. Golebiewski, *J. Chem. Phys.,* 1966, **45**, 2872.

[15] J. Simons and K. D. Jordan, *Chem. Rev.,* 1987, **87**, 535.

[16] K. D. Jordan and D. Burrow, *Chem. Rev.,* 1987, **87**, 557.

[17] J. Simons, *J. Phys. Chem. A,* 2008, **112**, 6401.

[18] J. Lecointre, G. M. Roberts, D. A. Horke and J. R. R. Verlet, *J. Phys. Chem. A,* 2010, **114**, 11216.

[19] D. A. Horke, G. M. Roberts, J. Lecointre and J. R. R. Verlet, *Rev. Sci. Instrum.,* 2012, **83**, 063101.

[20] A. T. J. B. Eppink and D. H. Parker, *Rev. Sci. Instrum.,* 1997, **68**, 3477.

[21] G. M. Roberts, J. L. Nixon, J. Lecointre, E. Wrede and J. R. R. Verlet, *Rev. Sci. Instrum.,* 2009, **80**, 053104.

[22] A. Amrein, R. Simpson and Hackett, *J. Chem. Phys.,* 1991, **94**, 4663.

[23] A. Amrein, R. Simpson and Hackett, *J. Chem. Phys.,* 1991, **95**, 1781.

[24] E. E. B. Campbell, G. Ulmer and I. V. Hertel, *Phys. Rev. Lett.,* 1991, **67**, 1986.

[25] B. Climen, F. Pagliarulo, A. Ollagnier, B. Baguenard, B. Concina, M. A. Lebeault, F. Lépine and C. Bordas, *Eur. Phys. J. D,* 2007, **43**, 85.

[26] M. W. Schmidt, K. K. Baldridge, J. A. Boatz, S. T. Elbert, M. S. Gordon, J. Jensen, S. Koseki, N. Matsunaga, K. A. Nguyen, S. Su, T. L. Windus, M. Dupuis and J. A. Montgomery, *J. Comput. Chem.,* 1993, **14**, 1347.

[27] R. Kendall, J. T. H. Dunning, Jr., and R. J. Harrison, *J. Chem. Phys.,* 1992, **96**, 6796.

[28] K. D. Jordan and F. Wang, *Annu. Rev. Phys. Chem.,* 2003, **54**, 367.

[29] M. Head-Gordon, J. A. Pople and M. J. Frisch, *Chem. Phys. Lett.,* 1988, **153**, 503.

[30] A. A. Granovsky, *J. Chem. Phys.,* 2011, **134**, 214113.

[31] J. Merrick, D. Moran and L. Radom, *J. Phys. Chem. A,* 2007, **111**, 11683.

[32] J. A. Pople, M. Head-Gordon and K. Raghavachari, *J. Chem. Phys.,* 1987, **87**, 5968.

[33] M. J. Frisch, G. W. Trucks, H. B. Schlegel, G. E. Scuseria, M. A. Robb, J. R. Cheeseman, G. Scalmani, V. Barone, B. Mennucci, G. A. Petersson, H. Nakatsuji, M. Caricato, X. Li, H. Hratchian, A. F. Izmaylov, J. Bloino, G. Zheng, J. L. Sonnenberg, M. Hada, M. Ehara, K. Toyota, R. Fukuda, J. Hasegawa, M. Ishida, T. Nakajima, Y. Honda, O. Kitao, H. Nakai, T. Vreven, J. J. A. Montgomery, J. E. Peralta, F. Ogliaro, M. Bearpark, J. J. Heyd, E. Brothers, K. N. Kudin, V. N. Staroverov, R. Kobayashi, J. Normand, K. Raghavachari, A. Rendell, J. C. Burant, S. S. Iyengar, J. Tomasi, M. Cossi, N. Rega, N. J. Millam, M. Klene, J. E. Knox, J. B. Cross, V. Bakken, C. Adamo, J. Jaramillo, R. Gomperts, R. E. Stratmann, O. Yazyev, A. J. Austin, R. Cammi, C. Pomelli, J. W. Ochterski, R. L. Martin, K. Morokuma, V. G. Zakrzewski, G. A. Voth, Salvador, J. J. Dannenberg, S. Dapprich, A. D. Daniels, Ö. Farkas, J. B. Foresman, J. V. Ortiz, J. Cioslowski and D. J. Fox, "Gaussian, Inc.," 2009.

[34] M. J. Bearpark, M. A. Robb and H. B. Schlegel, *Chem. Phys. Lett.,* 1994, **223**, 269.

[35] V. Barone, J. Bloino, M. Biczysko and F. Santoro, *J. Chem. Theory Comput.,* 2009, **5**, 540.

[36] E. Wigner, *Phys. Rev.,* 1948, **73**, 1002.

[37] K. J. Reed, A. H. Zimmerman, H. C. Andersen and J. I. Brauman, *J. Chem. Phys.,* 1976, **64**, 1368.

[38] R. N. Zare, *Mol. Photochem.,* 1972, **4**, 1.

[39] A. Sanov, *Annu. Rev. Phys. Chem.,* 2014, **65**, 341.

[40] J. Schiedt and R. Weinkauf, *J. Chem. Phys.,* 1999, **110**, 304.

[41] J. Simons, *J. Am. Chem. Soc.,* 1981, **103**, 3971.

[42] C. L. Adams, H. Schneider and J. M. Weber, *J. Phys. Chem. A,* 2010, **114**, 4017.

[43] Q. Fu, J. Yang and X.-B. Wang, *J. Phys. Chem. A,* 2011, **115**, 3201.

[44] B. Comita and J. I. Brauman, *J. Am. Chem. Soc.,* 1987, **109**, 7591.

[45] A. Modelli and D. Burrow, *J. Phys. Chem.,* 1984, **88**, 3550.

[46] A. A. Kunitsa and K. B. Bravaya, *J. Phys. Chem. Lett.,* 2015, **6**, 1053.

[47] O. G. Khvostenko, G. M. Tuimedov and U. M. Dzhemilev, *Doklady. Phys. Chem.,* 2007, **414**, 162.

[48] O. G. Khvostenko, V. G. Lukin and E. E. Tseplin, *Rapid. Commun. Mass Spectrom.,* 2012, **26**, 2535.

[49] D. A. Horke and J. R. R. Verlet, *Phys. Chem. Chem. Phys.,* 2011, **13**, 19546.

[50] G. M. Roberts, J. Lecointre, D. A. Horke and J. R. R. Verlet, *Phys. Chem. Chem. Phys.,* 2010, **12**, 6226.

[51] C. W. West, J. N. Bull, A. S. Hudson, S. L. Cobb and J. R. R. Verlet, *J. Phys. Chem. B,* 2015, **119**, 3982.

[52] C. W. West, A. S. Hudson, S. L. Cobb and J. R. R. Verlet, *J. Chem. Phys.,* 2013, **139**, 071104.